Escape Criterion Using Fixed Point Iteration with Applications in Fractal Generation

Sanjay Kumar Padaliya

Department of Mathematics, Shri Guru Ram Rai (Post Graduate) College, 248001, Dehradun, Uttarakhand, India. *Corresponding author*: spadaliya18@gmail.com

Saurabh Sharma

Department of Mathematics, Shri Guru Ram Rai (Post Graduate) College, 248001, Dehradun, Uttarakhand, India. E-mail: 75saurabhsharma@gmail.com

Gaurav Semwal

Department of Mathematics, Shri Guru Ram Rai (Post Graduate) College, 248001, Dehradun, Uttarakhand, India. E-mail: gsemwal281@gmail.com

Vijay Kumar

Department of Mathematics, Kirori Mal College, University of Delhi, 110007, Delhi, India. E-mail: vickyvijay000014@gmail.com

(Received on March 22, 2025; Revised on May 5, 2025 & May 19, 2025 & June 2, 2025 & June 12, 2025 & June 30, 2025; Accepted on July 3, 2025)

Abstract

This study employs the Picard-S3 iteration method, which proves to be particularly useful for visualizing and examining fractals, as well as investigating intricate dynamical systems. In the present paper, we focus on the complex polynomial function. By integrating numerical simulations with graphical representations, we explore how variations in iteration parameters affect the morphology and complexity of the obtained fractal structures. The findings indicate that different parameter values lead to highly intricate and diverse formations, highlighting the dynamic richness of these fractals. To systematically assess the effects of iteration parameters on fractal geometry, three quantitative measures are employed: Escape Time (ET), Density of Non-Escaping Points (DP), and Iteration Variance (IV). These metrics provide a thorough investigation on fractal structures respond to the parameter change, offering deeper insights into their dynamic properties and sensitivity to variations in iterative processes.

Keywords- Escape time, Fractals, Escape criterion, Density of non-escaping points, Iteration variance.

1. Introduction

Fractal are complex shaped patterns observed in both nature and Mathematics, a special class of self-similar patterns are called fractals in which fractal dimension strictly exceeds topological dimension of self-similar patterns (Weibel, 1991). These visually interesting and complex shapes appear in natural phenomena (Mandelbrot, 1982) such as branches of trees, snowflakes, and on the fern leaves (Barcellos, 1990). Mathematically, fractals are generated through iterative processes when a complex-valued function is repeatedly applied to produce self-similar patterns on different scales. Mandelbrot set is a fractal (Abbas et al., 2020) generated by iterating the function $f(z) = z^2 + c$, where $c \in C$. Similarly, the Julia set is also generated using the same function by varying initial conditions across the complex plane. Graphical depictions of these sets show the area, generating fractal patterns.



Fixed point theory provides an important framework to understand the iterative methods used in the visualization of fractals. The points that remain invariant under iteration and act as attractors, pulling nearby points toward them, are known as fixed points. In fractal dynamics, the term "escape" describes the behavior of points during iterations. Points escaping to infinity are assigned specific colors, while other points, escaping steadily or remaining bounded, are represented with different colors.

Mandelbrot sets are visualized using the escape time algorithm by different computer software like MATHEMATICA, MATLAB, Python, etc., calculating the total iterations required for a point's orbit to diverge to infinity. This approach showcases the dynamic nature of iterative processes in fractal generation. The Mandelbrot and Julia sets originated first in 1971, when the Picard iteration method was applied to the second-order polynomial, $f(z) = z^2 + c$. After these various iterative methods, such as Mann (Shahid et al., 2021) and Noor (Qi et al., 2020; Noor, 2000), are developed to explore diverse fractal patterns. These iterative methods provide insight for examining variations in the fractal properties, such as size, shape, and color, for different functions. Studies by various authors further expanded the understanding of fractals and their dynamic characteristics. Tomar et al. (2022a) used a sine function to generate fractals and revealed boundary patterns shaped by the complexities of transcendental dynamics. Husain et al. (2022), explored different types of fractals, showcasing their practical uses. Prajapati et al. (2022), use Mann iteration and uncover detailed and intricate fractal patterns. By suggesting a four-step iteration technique for weak contractions, Shatanawi et al. (2020) helped to enhance fixed-point calculations critical for fractal creation. Sharma et al. (2025) explore the potential of the Fibonacci sequence in fractal generation and show the symmetries of Mandelbrot and Julia sets mathematically by Fibonacci-Mann iteration. Antal et al. (2021) focused on the Fractals of complex sine function, revealing distinct behavior of iteration. Their 2022 followup brought Jungck-Ishikawa iteration equipped with s-convexity, which produced various fractals as Mandelbrot and Julia sets. Using the DK iteration, Sharma et al. (2023) obtained fractals for logarithmic function and Tassaddiq et al. (2023) key development was setting an original escape criteria for complex function-driven fractal, hence enhancing graphical representations. Tomar et al. (2023) also looked at cosine-based fractals and observed symmetrical patterns in both Mandelbrot and Julia forms. Introducing the Fibonacci-Mann iteration into transcendental contexts, Özgür et al. (2022) produced unique fractal shapes. Adhikari & Sintunavarat (2024) made logarithmic fractals more diverse and structured by using four-step iteration with s-convexity, which expanded the range even more. Comparing the resulting complexities in Mandelbrot sets, Srivastava et al. (2024) looked at Picard S-iteration to set escape criteria.

In this study, the Picard-S3 iteration method is applied to generate fractals for the complex polynomial $T(x) = x^r + ax + c$,

where, $c, a \in C$ and $r \ge 2$, the resulting Mandelbrot and Julia sets exhibit self-similar patterns identical to their classical structure. Analyzing these patterns provides insights into the mathematical behavior and dynamics of this class of complex functions. The fractals presented in this work highlight the dynamics of complex polynomial function under Picard-S3 iteration, offering valuable perspectives on their iterative properties. In 2022, Singh et al. (2022) introduced a three-step iteration method for approximation of fixed points in contraction mappings (Singh et al., 2022). This method, inspired by the Mann iterative scheme, demonstrates rapid convergence, makes it more effective for fractal generation.

The remainder of the paper is organized in the following manner: Section 2 provides key definitions, foundational concepts, and essential notations. Section 3 establishes an escape criterion for the function. In Section 4 Mandelbrot and Julia sets are generated for the Picard-S3 iteration, Section 5 provides numerical examples of fractal generation. and Section 6 summarizes the main findings and conclusions.

2. Preliminaries

Below are fundamental definitions and concepts that will be useful in this research.

Definition 2.1 Julia set (Barcellos, 1990; Julia, 1918): The Julia set is defined as the collection of all points within the complex plane for which the orbit of the function $T: C \to C$ diverges to infinity. The filled Julia set of T can be expressed as:

$$S_T = \{x \in C : \{ |T^i(x)| \}_{i=0}^{\infty} \text{ is bounded} \}$$

$$\tag{1}$$

The boundary of S_T is referred to as the Julia set of T.

Definition 2.2 Mandelbrot set (Devaney, 2018): The Mandelbrot set is the set of parameter values c within the complex plane such that the filled Julia set S_T , corresponding to the function $T(x) = x^2 + c$, is connected. Formally, it is defined as:

$$M_S = \{c \in C: S_T \text{ is connected }\}$$
 (2)

The Mandelbrot set M_S encapsulates significant information about the filled Julia set and can alternatively be expressed as:

$$M_S = \{ |T(x)| \to \infty \text{ as } k \to \infty \}$$
 (3)

Definition 2.3 Picard-S3 iteration (Singh et al., 2022): For $x_0 \in C$, Picard-S3 iteration is defined as

$$y_{i} = (1 - \alpha_{i})x_{i} + \alpha_{i}T(T(x_{i})),$$

$$x_{i+1} = (1 - \beta_{i})y_{i} + \beta_{i}T(y_{i})$$
(4)

where, $\alpha_i, \beta_i \in (0,1]$ and i = 0,1,2...

3. Main Results

Escape criteria play an important role in the visualization of complex fractals. In this work, we establish the escape criteria for the given function using the Picard-S3 iteration. The Picard-S3 iteration consists of two steps, where we consider the sequences $\alpha_i = \alpha$ and $\beta_i = \beta$.

3.1 Escape Criteria of Picard-S3 Iteration

Suppose $T(x) = x^r + ax + c$, where $c, a \in C$, and $r \ge 2$, be a function, then,

Theorem 3.1 Let $T(x) = x^r + ax + c$, where $c, a \in C$ and $r \ge 2$ and $\{x_i\}_{i \in W}$ be the Picard-S3 iteration defined in Equation (4). If, $|x_0| \ge |c| > (2 + |a|)^{\frac{1}{(r-1)}}$, $|x_0| \ge |c| > \left(\frac{2-\alpha}{\alpha}\right)^{\frac{1}{(r-1)}}$ and $|x_0| \ge |c| > \left(\frac{2+\beta|a|}{\beta}\right)^{\frac{1}{(r-1)}}$. Then $|x_i| \to \infty$, as $i \to \infty$.

Proof. From Equation (4), the initial step of Picard-S3 iteration is,

$$|y_i| = |(1 - \alpha)x_i + \alpha T(T(x_i))|$$

Then for i = 0 and from $T_c(x) = x^r + ax + c$, we get, $|y_0| = |(1 - \alpha)x_0 + \alpha T(T(x_0))|$ $= |(1 - \alpha)x_0 + \alpha T(x_0^r + ax_0 + c)|.$

So, we get,

$$|y_{0}| = |(1 - \alpha)x_{0} + \alpha[(x_{0}^{r} + ax_{0} + c)^{r} + a(x_{0}^{r} + ax_{0} + c) + c]|$$
Since $|x_{0}| \ge |c|$, then for large $|x_{0}|$, the term $|x_{0}|^{r}$ dominates in $T(x_{0})$ so,
$$|T(x_{0})| = |x_{0}^{r} + ax_{0} + c|$$

$$\ge |x_{0}|^{r} - |a||x_{0}| - |c|$$
 (By using triangle inequality).

From $|x_0| \ge |c|$, we have,

$$|T(x_0)| \ge |x_0|^r - |a||x_0| - |x_0|$$

= |x_0|(|x_0|^{r-1} - |a| - 1).

Since $|x_0| > (2+|a|)^{\frac{1}{r-1}}$, we have $|x_0|^{r-1} > 2+|a|$, it follows that $|x_0|^{r-1}-|a|-1>1$, so, $|T(x_0)| \ge |x_0|(|x_0|^{r-1}-|a|-1)>|x_0|$.

Next, we compute,

$$T(T(x_0) = T(x_0^r + ax_0 + c) = (x_0^r + ax_0 + c)^r + a(x_0^r + ax_0 + c) + c.$$

To bound $|T(T(x_0))|$, applying the triangle inequality,

$$|T(T(x_0))| \ge |(x_0^r + ax_0 + c)^r| - |a(x_0^r + ax_0 + c)| - |c|$$
(6)

Since $|x_0^r + ax_0 + c| \ge |x_0|^r - |a||x_0| - |c|$, we have,

$$|(x_0^r + ax_0 + c)^r| \ge (|x_0|^r - |a||x_0| - |c|)^r \ge (|x_0|^r - |a||x_0| - |x_0|)^r (: |x_0| \ge |c|) = |x_0|^r (|x_0|^{r-1} - |a| - 1)^r$$
(7)

For the second term,

$$|a(x_0^r + ax_0 + c)| \le |a|(|x_0|^r + |a||x_0| + |c|) \le |a|(|x_0|^r + |a||x_0| + |x_0|).$$
(8)

Substituting Equation (7) and Equation (8) into Equation (6), we get,

$$|T(T(x_0))| \ge |x_0|^r (|x_0|^{r-1} - |a| - 1)^r - |a|(|x_0|^r + |a||x_0| + |x_0|) - |c| \tag{9}$$

To simplify, factor out $|x_0|$,

$$|x_0|^r (|x_0|^{r-1} - |a| - 1)^r = |x_0|^{r^2} \left(1 - \frac{|a| + 1}{|x_0|^{r-1}}\right)^r,$$

$$|a|(|x_0|^r + |a||x_0| + |x_0|) = |a||x_0|^r \left(1 + \frac{|a| + 1}{|x_0|^{r-1}}\right).$$

Thus Equation (9) becomes.

$$\left| T(T(x_0)) \right| \ge |x_0|^{r^2} \left(1 - \frac{|a|+1}{|x_0|^{r-1}} \right)^r - |a||x_0|^r \left(1 + \frac{|a|+1}{|x_0|^{r-1}} \right) - |c|
\left| T(T(x_0)) \right| \ge |x_0| \left[|x_0|^{r^2-1} \left(1 - \frac{|a|+1}{|x_0|^{r-1}} \right)^r - |a|(|x_0|^{r-1} + |a|+1) - \frac{|c|}{|x_0|} \right]$$
(10)

For large $|x_0|$, since $|x_0|^{r-1} > 2 + |a|$, the term $\frac{|a|+1}{|x_0|^{r-1}} < 1$. Also $|a|(|x_0|^{r-1} + |a| + 1) \approx |a||x_0|^{r-1}$, and $\frac{|c|}{|x_0|} \le 1$. Thus,

$$|T(T(x_0))| \ge |x_0| (|x_0|^{r^2 - 1} - |a||x_0|^{r - 1} - |a| - 1)$$

$$= |x_0|^r (|x_0|^{r + 1} - |a| - \frac{|a| + 1}{|x_0|^{r - 1}}).$$
(11)

Since
$$\frac{|a|+1}{|x_0|^{r-1}} < 1$$
,
 $|T(T(x_0))| \ge |x_0|^r (|x_0|^{r+1} - |a| - 1)$ (12)

Now,

$$|x_0|^{r+1} > |x_0|^{r-1} \quad (\because r \ge 2)$$

> 2 + |a| \quad (\text{:} \quad |x_0| > (2 + |a|)\frac{1}{(r-1)})

Hence Equation (12) becomes,

$$\left|T(T(x_0))\right| \ge |x_0|^r \tag{13}$$

Using Equation (13) in Equation (5) we get,

$$|y_0| = |(1 - \alpha)x_0 + \alpha T(T(x_0))|$$

$$= |\alpha T(T(x_0)) + (1 - \alpha)x_0|$$

$$\geq \alpha |T(T(x_0))| - (1 - \alpha)|x_0|$$

$$\geq \alpha |x_0|^r - (1 - \alpha)|x_0|$$

$$\geq |x_0|(\alpha|x_0|^{r-1} - (1 - \alpha)).$$

Since $|x_0| \ge \left(\frac{2-\alpha}{\alpha}\right)^{\frac{1}{r-1}}$, and $r \ge 2$, we have $|x_0|^{r-1} \ge \frac{2-\alpha}{\alpha}$.

Thus,

$$|y_0| \ge |x_0| \tag{14}$$

In the next step of Picard-S3 iteration,

$$|x_{i+1}|=|(1-\beta_i)y_i+\beta_i T(y_i)|$$

for i = 0 we have,

$$\begin{aligned} |x_1| &= |(1-\beta)y_0 + \beta T(y_0)| \\ &= |(1-\beta)y_0 + \beta(y_0^r + ay_0 + c)| \\ &\geq |\beta y_0^r + \beta ay_0 + \beta c)| - (1-\beta)|y_0| \\ &\geq \beta|y_0^r| - \beta|a||y_0| - \beta|c| - (1-\beta)|y_0|. \end{aligned}$$

The assumption $|y_0| \ge |c|$ implies $-|c| \ge -|y_0|$, therefore we get,

$$\begin{aligned} |x_1| &\geq \beta |y_0^r| - \beta |a| |y_0| - \beta |y_0| - (1 - \beta) |y_0| \\ &= \beta |y_0^r| - \beta |a| |y_0| - |y_0| \\ &= |y_0| (\beta |y_0^{r-1}| - \beta |a| - 1). \end{aligned}$$

From Equation (14), we have,

$$|x_1| \ge |x_0| \left(\beta \left| x_0^{r-1} \right| - \beta |a| - 1\right).$$

Since
$$|x_0| \ge |c| > \left(\frac{2+\beta|a|}{\beta}\right)^{\frac{1}{(r-1)}} \Longrightarrow \left(\beta \left|x_0^{r-1}\right| - \beta|a| - 1\right) > 1$$
,

Therefore,

$$|x_1| \ge |x_0|$$
.

Now using the same argument recursively,

For i = 1,

$$|x_2| \ge |x_0| (\beta |x_0^{r-1}| - \beta |a| - 1)^2 \Longrightarrow |x_2| > |x_0|.$$

Next, for i = 2, we have,

$$|x_{3}| \ge |x_{0}| (\beta |x_{0}^{r-1}| - \beta |a| - 1)^{3}.$$

$$\vdots$$

$$|x_{i+1}| \ge |x_{0}| (\beta |x_{0}^{r-1}| - \beta |a| - 1)^{i}.$$

Therefore, $|x_i| \to \infty$ as $i \to \infty$.

Remark 1. The condition $|x_0| \ge |c| > \max\left\{ |c|, (2+|a|)^{\frac{1}{r-1}}, \left(\frac{2-\alpha}{\alpha}\right)^{\frac{1}{r-1}}, \left(\frac{2+\beta|a|}{\beta}\right)^{\frac{1}{r-1}} \right\}$, ensure $|x_0|^{r-1}$ is sufficiently large to make the dominant terms (e.g., $|x_0|^{r^2}$, $|y_0|^{r-1}$) outweigh lower-order terms, validating the approximations. Specifically:

- $|x_0|^{r-1} > 2 + |a|$ ensures $|x_0|^{r^2-1} > |a| + 2$, so $|T(T(x_0))| > |x_0|$.
- $|x_0|^{r-1} > \frac{2-\alpha}{\alpha}$ ensure $|y_0| \approx \alpha |x_0|^{r^2} > |x_0|$.
- $|x_0|^{r-1} > \frac{\alpha}{\beta}$ ensure $|x_1| > |y_0|$.

Corollary 3.1 For $k \geq 0$, if

$$\{|x_{i}| > x_{0} > \max\{|c|, (2+|a|)^{\frac{1}{(r-1)}}, \left(\frac{2-\alpha}{\alpha}\right)^{\frac{1}{(r-1)}}, \left(\frac{2+\beta|a|}{\beta}\right)^{\frac{1}{(r-1)}}\}\} \ , \ \ then \ \ there \ \ exists \ \theta > 0, \ so \ \ that \\ |x|\left(\left(\left|x_{0}^{r-1}\right| - |a| - 1\right)\left(\alpha\left|x_{0}^{r-1}\right| - 1 + \alpha\right)\left(\beta\left|x_{0}^{r-1}\right| - \beta|a| - 1\right)\right) > 1 + \theta \Longrightarrow |x_{k+i}| > |x_{k}|(1+\theta)^{k+i} \ and \ then \ |x_{i}| \to \infty \ as \ i \to \infty.$$

4. Generation of Fractals for $T(x) = x^r + ax + c$

To generate Julia sets, we employ Algorithm 1, while Algorithm 2 is utilized for Mandelbrot sets. These algorithms are implemented to construct fractals for the polynomial function using the Picard-S3 iteration scheme in MATLAB (R2015a) with an appropriate colormap (**Figure 1**) and different value of parameters (**Table 1-4**). Throughout this iterative process, a diverse range of fractals emerges, representing Julia and Mandelbrot sets. To ensure consistency across numerical experiments, the Picard-S3 parameters $\alpha, \beta \in (0,1]$ are sampled over resolution grid.

The coloring algorithm maps the number of Picard-S3 iterations i before an orbit escape to a color index. For each point x_0 (Julia set) or c (Mandelbrot set), the orbit escapes when $|x_{i+1}| > R$ or $|z_{i+1}| > R$, respectively. The color index j is computed as

$$j = \left| (C - 1) \frac{i}{p} \right|,$$

where, C is the number of colors in the colormap, and P is the maximum iteration count. Points that remain bounded after P iterations (i.e., i = P) are assigned the last color, indicating potential membership in the set. Notably, many of these fractals exhibit symmetrical properties. This self-similarity holds considerable significance, particularly in applications such as the Textile Industry and interior design, where such patterns are prized for their intricate structures and visual appeal.

4.1 Julia Sets

We generate the Julia sets for the polynomial function $T(x) = x^r + ax + c$, where $c, a \in C$ and $r \ge 2$, by varying the parameter values using the Picard-S3 iteration method. The maximum number of Picard-S3 iteration, P is set to 30.

Figure 1. Colourmap for the fractals.

Algorithm 1: Generation of Julia Set

Input: $T(x) = x^r + ax + c$, where $c, a \in C$ and $r \ge 2$; $Area A \subset C$; P Maximum iterations;

 $\alpha, \beta \in (0,1]$; Color map[0...C-1] with C colors

Output: Julia set for area A

1) for each $x_0 \in A$ do

2)
$$R = \max \left\{ |c|, (2+|a|)^{\frac{1}{r-1}}, \left(\frac{2-\alpha}{\alpha}\right)^{\frac{1}{r-1}}, \left(\frac{2+\beta|a|}{\beta}\right)^{\frac{1}{r-1}} \right\}$$

- 3) i = 0
- 4) $x_i = x_0$
- 5) while $i \leq P do$
- 6) $y_i = (1 \alpha)x_i + \alpha T^2(x_i)$
- 7) $x_{i+1} = (1 \beta)y_i + \beta T(y_i)$
- 8) if $|x_{i+1}| > R$ then
- 9) break
- 10) end if
- 11) i = i + 1
- 12) end while

$$13) j = \left| (C-1) \frac{i}{P} \right|$$

- 14) Color x_0 with Color map[j]
- 15) end for

Table 1. Parametric values used in **Figure 2** for Julia sets.

Sr. No.	α	β	а	r	Area	Time
(a)	0.99	1	0.583-0.785i	2	[-1.3,0.7]× [-0.8,1.6]	1.279249s.
(b)	0.99	1	0.583-0.785i	3	[-1.2,1.2]× [-1.5,1.5]	2.516655s.
(c)	0.99	1	0.583-0.785i	4	[-1.2,1.2]× [-1.3,1]	2.602523s.
(d)	0.99	1	0.583-0.785i	5	[-1.2,1.2]× [-1.2,1.2]	2.733305s.
(e)	0.99	1	0.583-0.785i	6	[-1.2,1.2]× [-1.2,1.2]	2.919975s.
(f)	0.99	1	0.583-0.785i	7	[-1.2,1.2]× [-1.2,1.2]	2.998813s.

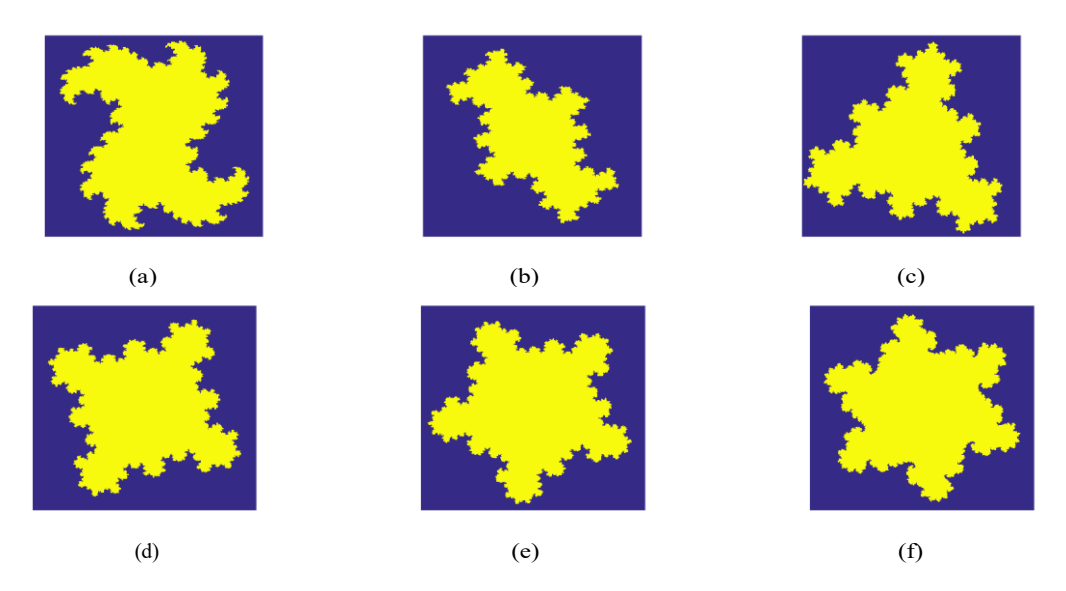


Figure 2. Julia sets for Picard-S3 iteration.

In **Figures 2 (a)-(f),** $c = \frac{0.9}{100}i$, and combination of parameters given in **Table 1** is used and examine that Julia sets appear for this exponential function appear like the subclasses of complex starlike function found in different symmetrical shapes in Geometry and Biological world.

Table 2. Parametric values used in Figure 3 for Julia sets.

Sr. No.	α	β	а	r	Area	Time
(a)	0.1	0.8	0.1	2	[-2.5,1.6]× [-2.5,2.5]	1.357802s.
(b)	0.1	0.8	0.1	3	[-1.3,1.3]× [-1.4,1.4]	2.075251s.
(c)	0.1	0.8	0.1	4	[-1.3,1.3]× [-1.4,1.4]	3.013689s.
(d)	0.25	0.89	0.1	2	[-2,1.2]× [-1.8,1.8]	1.272235s.
(e)	0.25	0.89	0.5	2	[-2,1]× [-1.8,1.8]	1.265864s.
(f)	0.25	0.89	1	2	[-2.2.0.8]× [-1.8.1.8]	1.272035s.

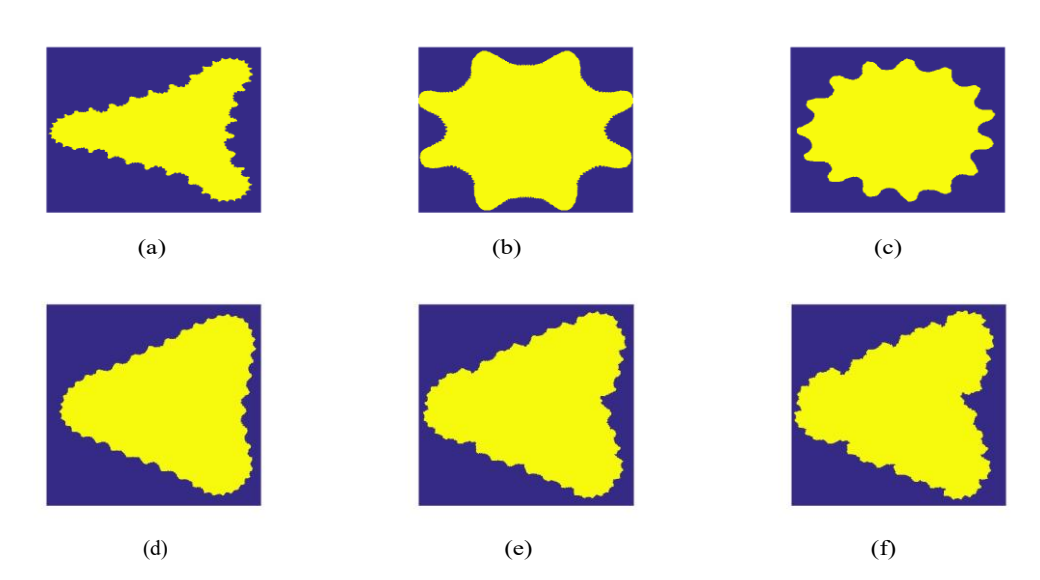


Figure 3. Julia sets for Picard-S3 iteration.

In Figure 3(a)-(f), c = 0.1i, and combination of parameters given in Table 2 is used and Julia fractals approach sunflower shapes with circular symmetry as the value of r increases. And for higher values of r Julia fractals approach triangular shapes with non-rectifiable boundary (See Figure 3).

4.2 Mandelbrot Set

In this section, we examine different Mandelbrot sets for the function $T(x) = x^r + ax + c$, where $c, a \in C$ and $r \ge 2$, for distinct values of r within the orbit of the Picard-S3 iteration. Mandelbrot sets have been generated for various parameter configurations using the Picard-S3 iteration method. To ensure uniformity across all fractals, the maximum number of iterations, P is fixed at 30 as specified in Algorithm 2.

Algorithm 2: Generation of Mandelbrot Set

Input: $T(x) = x^r + ax + c$, where $c, a \in C$ and $r \ge 2$; $Area A \subset C$; Maximum iterations P; $\alpha, \beta \in (0,1]$; Color map[0...C-1] with C colors

Output: Mandelbrot set for area A

1) for each $c \in A$ do

2)
$$R = \max \left\{ |c|, (2 + |a|)^{\frac{1}{r-1}}, \left(\frac{2-\alpha}{\alpha}\right)^{\frac{1}{r-1}}, \left(\frac{2+\beta|a|}{\beta}\right)^{\frac{1}{r-1}} \right\}$$

- 3) i = 0
- 4) $x_i = 0$
- 5) while $i \leq P do$
- 6) $y_i = (1 \alpha)x_i + \alpha T^2(x_i)$

7)
$$x_{i+1} = (1 - \beta)y_i + \beta T(y_i)$$

- 8) if $|x_{i+1}| > R$ then
- 9) break
- 10) end if
- 11) i = i + 1
- 12) end while

$$13) j = \left| (C-1) \frac{i}{p} \right|$$

- 14) Color c with Color map[j]
- 15) end for

Table 3. Parametric values used in Figure 4 for Mandelbrot sets.

Sr. No.	α	β	а	r	Area	Time
(a)	0.9	0.1	0.1	2	[-1.5,1.6]× [-1,1]	1.609162s.
(b)	0.9	0.2	0.1	2	[-1.5,0.6]×[-1,1]	1.509401s.
(c)	0.9	0.5	0.1	2	[-1.5,0.6]× [-1,1]	1.563076s.
(d)	0.9	0.6	0.5	2	[-1.5,0.6]×[-1,1]	1.648927s.
(e)	0.9	0.8	0.5	2	[-1.5,0.6]×[-1,1]	1.684885s.
(f)	0.9	0.1	0.5	2	[-2.2,0.8]×[-1.8,1.8]	1.673943s.

Table 4. Parametric values used in **Figure 5** for Mandelbrot sets.

Sr. No.	α	β	а	r	Area	Time
(a)	0.99	0.98	0.5	4	[-1,0.7]× [-0.8,0.8]	3.026923s.
(b)	0.99	0.98	0.5	5	[-0.7,0.7]× [-0.7,0.7]	2.966343s.
(c)	0.99	0.98	0.5	7	[-0.7,0.7]× [-0.7,0.7]	3.375605s.
(d)	0.99	0.98	0.5	8	[-0.7,0.7]× [-0.7,0.7]	4.170721s.
(e)	0.99	0.98	0.5	11	[-0.7,0.7]× [-0.7,0.7]	4.781605s.
(f)	0.99	0.98	0.5	15	[-0.7,0.7]×[-0.7,0.7]	5.177218s.

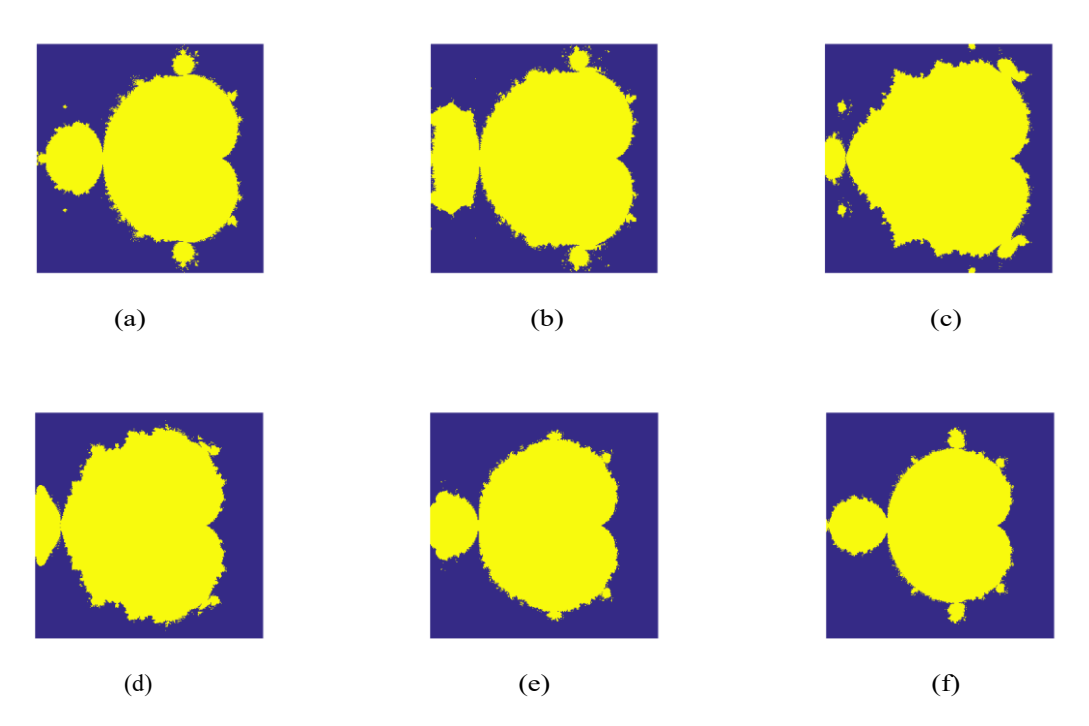


Figure 4. Mandelbrot sets for Picard-S3 iteration.

Mandelbrot Sets appear in **Figure 4 (a)-(f)**, with bean shaped portion. For higher values of r and value of parameters given in **Table 3** it closely resembles to original Mandelbrot set given by Benoit Mandelbrot.

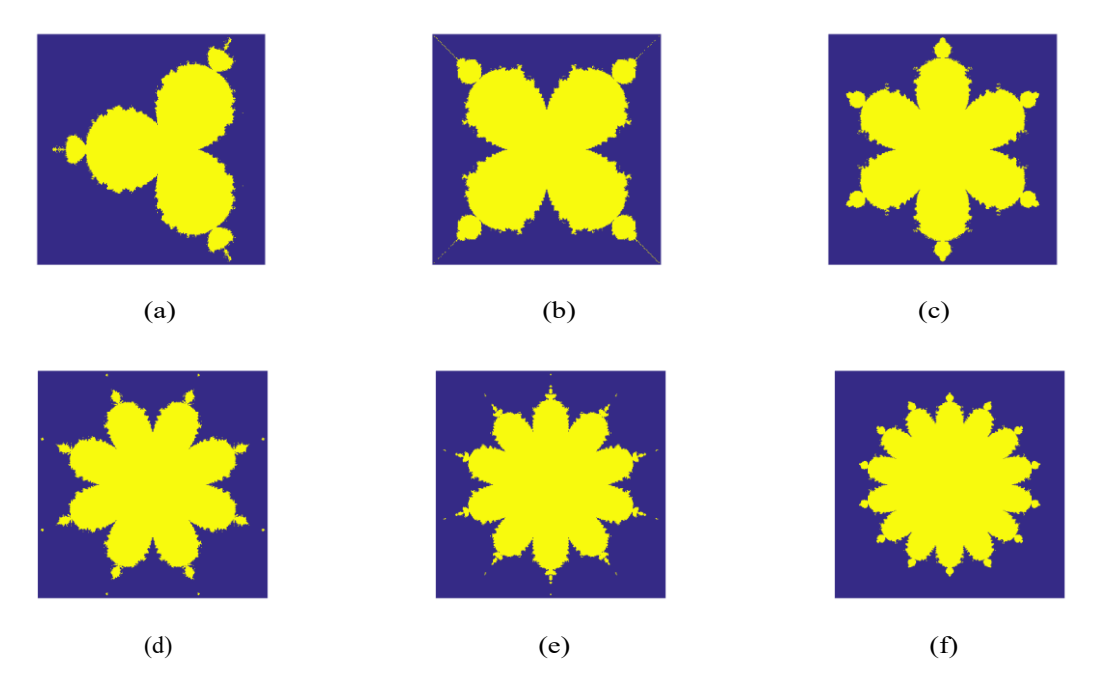


Figure 5. Mandelbrot sets for Picard-S3 iteration.

Mandelbrot sets for higher values of r is obtained. The set approach's petal like shapes with circular symmetry (See Figures 5 (a)-(f) and Table 4).

Figures 2-5, shows that the computation time is significantly less than the standard fixed-point iterations such as Picard, Mann, Ishikawa, etc. For r = 2, generated fractal closely resembles the classical Mandelbrot set (See **Figure 4(a)** and **Figure 4(f)**), which show the efficiency of the Picard-S3 iteration.

5. Numerical Examples

In this section, we analyze the Mandelbrot and Julia sets for polynomial functions via the Picard-S3 iteration. The Mandelbrot sets for complex polynomial functions typically forms a petal-like shape. This section investigates the influence of various parameters on the Julia and Mandelbrot sets. Different metrics are employed to better understand these effects on the sets, allowing us to represent different properties graphically. We compute three key measures namely, Escape Time (ET), Density of Non-Escaping Points (DP), and Iteration Variance (IV). These metrices are obtained from distinct points in the set. The Escape Time (ET) quantifies the mean iterations required for points in the complex plane to escape from a bounded region:

$$ET = \frac{1}{N_{\text{esc}}} \sum_{i \in \text{Escaping Points}} k_i,$$

where, N_{esc} denotes the total number of points that escape within the maximum iteration limit, and k_i represents the iteration count needed for the i^{th} point to escape. If no points escape, the escape time is generally set to the maximum iteration limit. The Density of Non-Escaping Points (DP) assesses the proportion of points inside fractal that remain bounded after the maximum number of iterations:

$$DP = \frac{N_{\text{non-esc}}}{N_{\text{total}}},$$

where, $N_{\text{non-esc}}$ is the number of points that did not escape, and N_{total} is the total points in the grid. Iteration Variance (IV) is a statistical measure that evaluates the variability in the iterations required for points to either escape or remain within the fractal.

$$IV = \frac{1}{N} \sum_{i=1}^{N} \left(k_i - \bar{k} \right)^2,$$

where, k_i is the iteration count for the i^{th} point, \bar{k} is the average iteration count, and N represents the number of points. To illustrate the relation between the parameters α and β with these numerical measures, we analyze the Mandelbrot and Julia sets for distinct values of a and r. These measures are calculated and the final outcomes are plotted. The parameters α and β are sampled at 100 points which are evenly spaced within the range (0,1], resulting in 10,000 generated images for each plot from **Figure 6** to **Figure 15**.

5.1 ET, DP and IV for Julia Sets

In **Figure 6**, the plots for the measures of Escape Time (ET), Density of Non-Escaping Points (DP), and Iteration Variance (IV) are shown for the function $T(x) = x^r + ax + c$. The maximum iteration count is set to 30, with $c = \frac{0.9}{100}i$, r = 2, and a = 0.583 - 0.785i. The image generated in the area $[-2,2]^2$. By examining the plots, it is observed that the highest ET value is 24.6227, at $\alpha = 1.0$ and $\beta = 0.01$, while the lowest ET value of 0.6088 is observed at $\alpha = 0.1$ and $\beta = 0.5$. In contrast, the DP plot displays a distinct pattern contrast to the ET measure. The peak DP value is 0.7569, which occurs at $\alpha = 1.0$ and $\beta = 1.0$, while

the lowest DP value of 0 is observed at several different α and β values. The plots for DP and IV share similar trends. The highest IV value is 216.2349, occurring at $\alpha = 0.25$ and $\beta = 0.34$, while the lowest IV value of 14.2744 is observed at $\alpha = 0.01$ and $\beta = 0.05$. **Figure 6**, clearly demonstrates that both the ET and DP measures attain highest values at the boundaries.

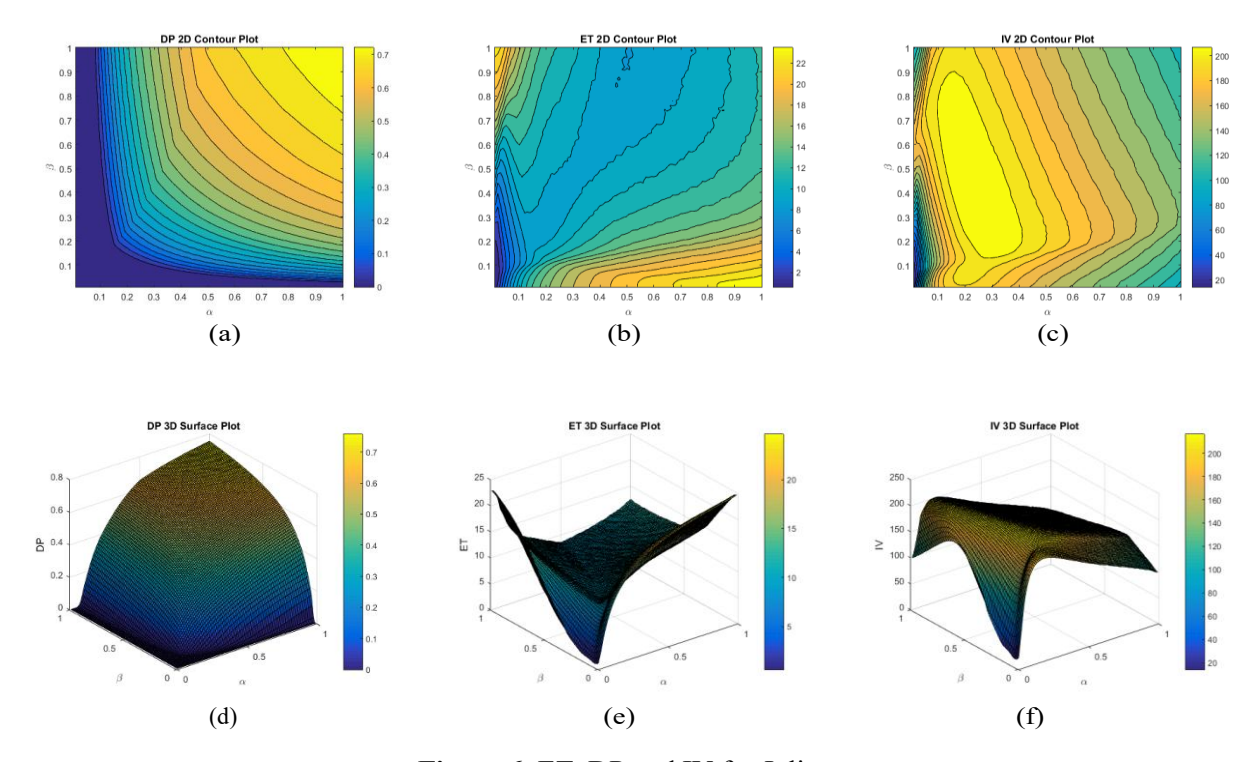


Figure 6. ET, DP and IV for Julia sets.

In **Figure 7**, the Escape Time (ET), Density of Non-Escaping Points (DP), and Iteration Variance (IV) measures plots are shown for the function $T(x) = x^r + ax + c$ with parameters $c = \frac{0.9}{100}i$, r = 5, and a = 0.583 - 0.785i. From plots, the highest ET value is 9.1325, which occurs at $\alpha = 0.01$ and $\beta = 0.99$, while the lowest ET value is 0.6035, seen at $\alpha = 0.82$ and $\beta = 0.69$. In contrary, the DP plot displays a different trend to the ET measure. The highest DP value is 0.8418, which occurs at $\alpha = 1.0$ and $\beta = 1.0$, while the lowest DP value is 0.7032, observed at $\alpha = 0.01$ and $\beta = 0.01$. The plots for DP and IV show similar behaviors. The highest IV value is 171.7265, occurring at $\alpha = 0.01$ and $\beta = 0.07$, while the lowest IV value of 111.2017 is observed at $\alpha = 1.0$ and $\beta = 1.0$. **Figure 7**, offers a detailed analysis of these measures.

In **Figure 8**, the Escape Time (ET), Density of Non-Escaping Points (DP), and Iteration Variance (IV) measures are shown for the parameters c = 0.1i, a = 0.1, and r = 2. Upon reviewing the plots, the highest ET value of 23.2318 is observed at $\alpha = 1.0$ and $\beta = 0.01$, while the lowest ET value of 0.2471 occurs at $\alpha = 0.01$ and $\beta = 0.03$. In contrast to the ET measure, the DP plot demonstrates a distinct pattern. The maximum value for DP measure is 0.7697, for $\alpha = 1.0$ and $\beta = 1.0$, and the minimum value for DP measure is 0, for multiple combinations of α and β . The plots of DP and IV on comparison show distinct behavior. The highest IV value of 216.9689 occurs at $\alpha = 0.29$ and $\beta = 0.35$, and the lowest IV value of 5.2816 is recorded at $\alpha = 0.01$ and $\beta = 0.03$.

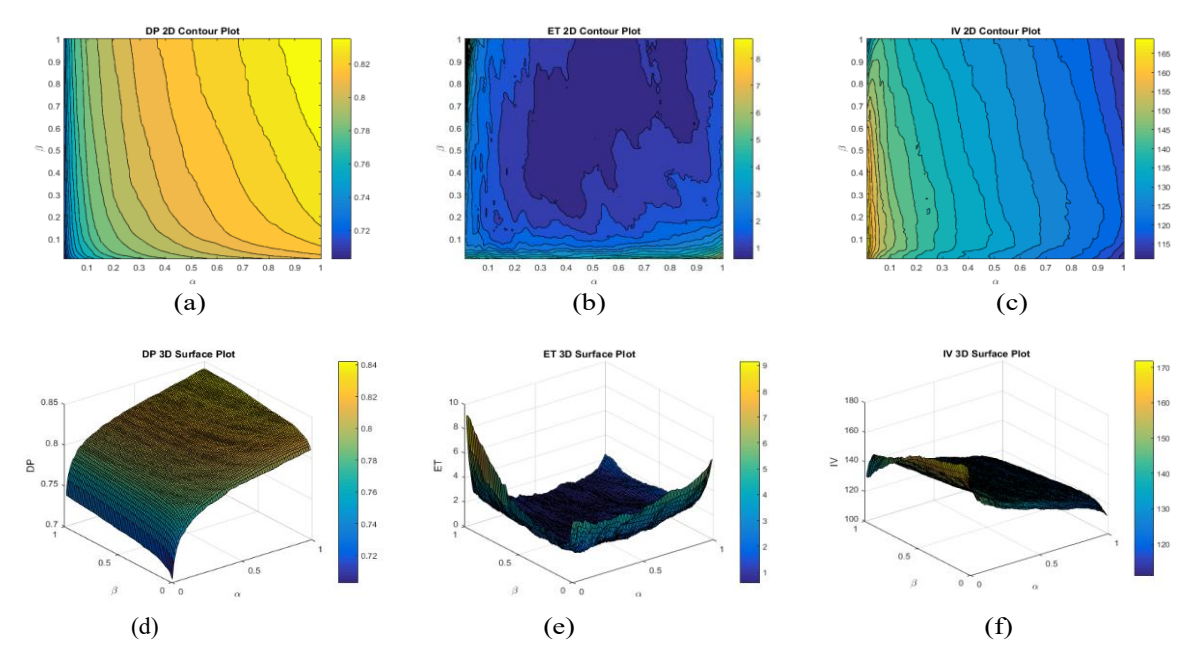


Figure 7. ET, DP and IV for Julia sets.

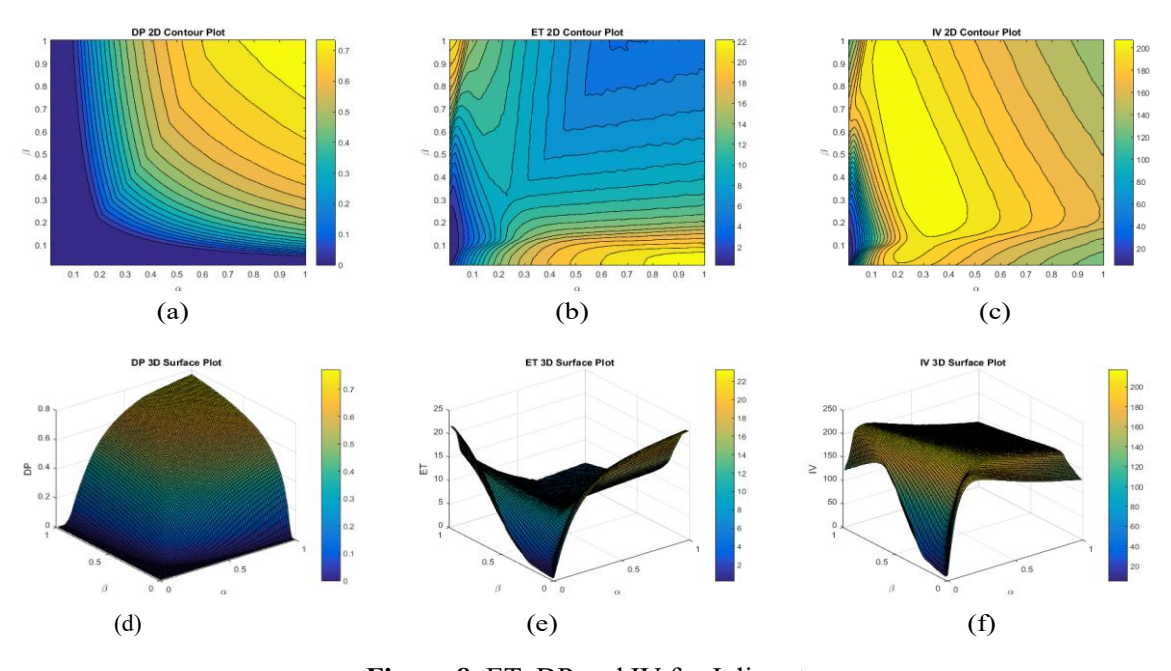


Figure 8. ET, DP and IV for Julia sets.

In **Figure 9**, the plots for the Escape Time (ET), Density of Non-Escaping Points (DP), and Iteration Variance (IV) measures are for the parameters c = 0.1i, a = 0.1, and r = 4. The plots reveal that the maximum ET value is 9.4477 occurs at $\alpha = 0.01$ and $\beta = 1$, while the upper limit of ET value is 0.1441, observed at $\alpha = 0.74$ and $\beta = 0.87$. The DP plot, shows a different behavior contrast to the ET measure. The highest DP value, 0.8072, is at $\alpha = 1.0$ and $\beta = 1.0$, whereas the minimum DP value of 0.5886 occurs at $\alpha = 0.01$ and β

= 0.01. The behavior of the DP and IV plots is similar. The highest IV value of 199.3113 appears at α = 0.01 and β = 0.07, while the lowest IV value of 139.1188 is recorded at α = 1.0 and β = 1.0.

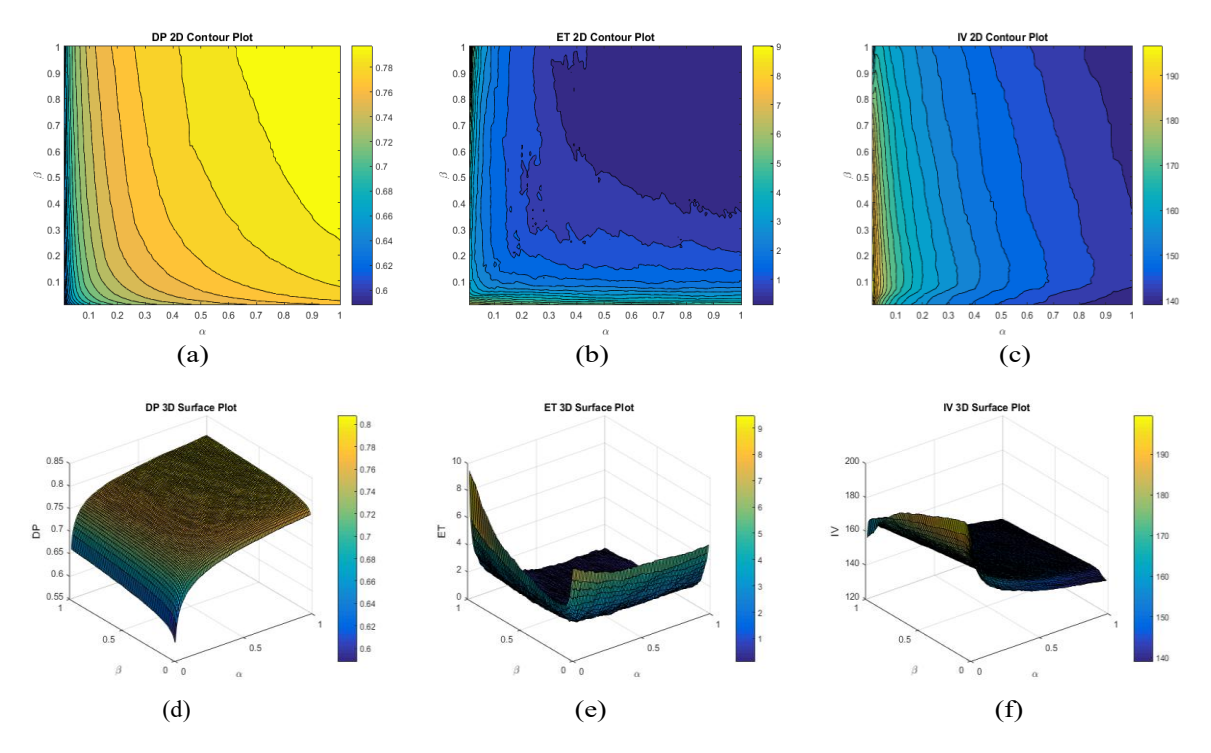


Figure 9. ET, DP and IV for Julia sets.

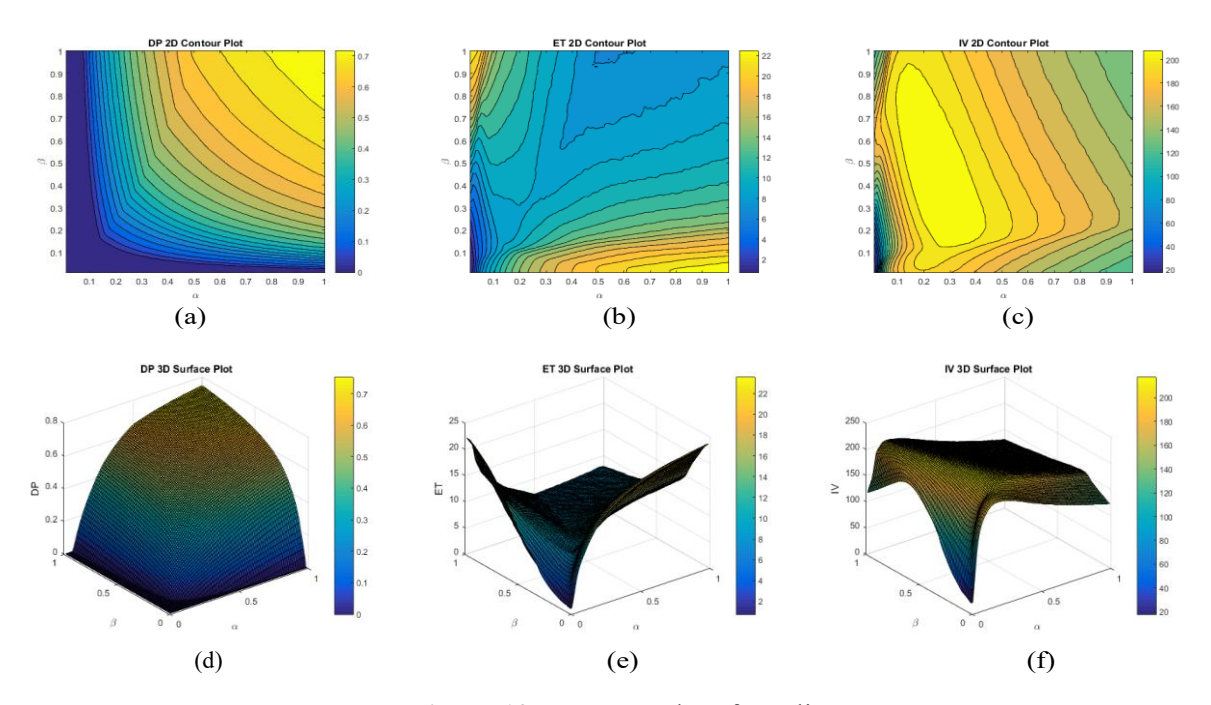


Figure 10. ET, DP and IV for Julia sets.

In **Figure 10**, the Escape Time (ET), Density of Non-Escaping Points (DP), and Iteration Variance (IV) plots displayed for the combination of parameters c=0.1i, a=1, and r=2. The plots shows that the Maximum ET value is 23.5441, for $\alpha=1.0$ and $\beta=0.01$, while the minimum ET value is 0.7610, for $\alpha=0.01$ and $\beta=0.03$. The DP plot, is different to the ET measure. The highest value for DP measure is 0.7517, for $\alpha=1.0$ and $\beta=1.0$, while the minimum value for DP measure is 0 observed for multiple combinations of α and β . The plot for DP and IV measures shows similar patterns. The highest IV value of 217.0 occurs at $\alpha=0.27$ and $\beta=0.36$, whereas the lowest IV value of 17.8503 is found at $\alpha=0.01$ and $\beta=0.03$.

5.2 ET, DP and IV Measures for Mandelbrot Sets

In **Figure 11**, the plots for Escape Time (ET), Density of Non-Escaping Points (DP), and Iteration Variance (IV) measures are presented for the combination of the parameters a = 0.1, and r = 2. We get the highest ET value of 25.5502 occurs at $\alpha = 1.0$, $\beta = 0.01$, while the minimum ET value of 0.6476 is found at $\alpha = 0.01$, $\beta = 0.04$. The DP measure plot present different pattern in contrast to the ET measure. The highest DP value is 0.7968, for $\alpha = 1.0$, $\beta = 1.0$, while the lowest DP value is 0, observed for various combinations of α and β . Both the DP and IV measure plots show similar patterns. The maximum IV value of 215.0777 occurs at $\alpha = 0.25$, $\beta = 0.29$, while the minimum IV value of 15.0110 is observed at $\alpha = 0.01$, $\beta = 0.03$.

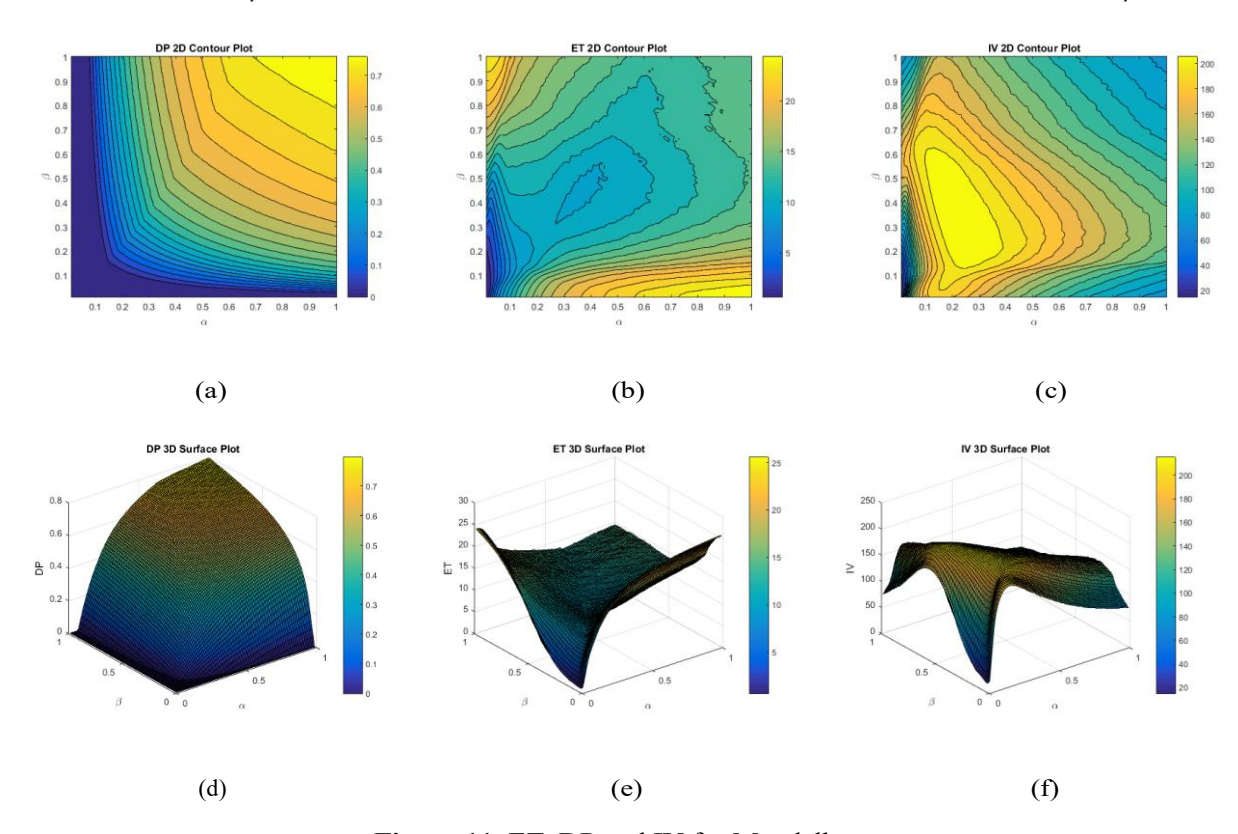
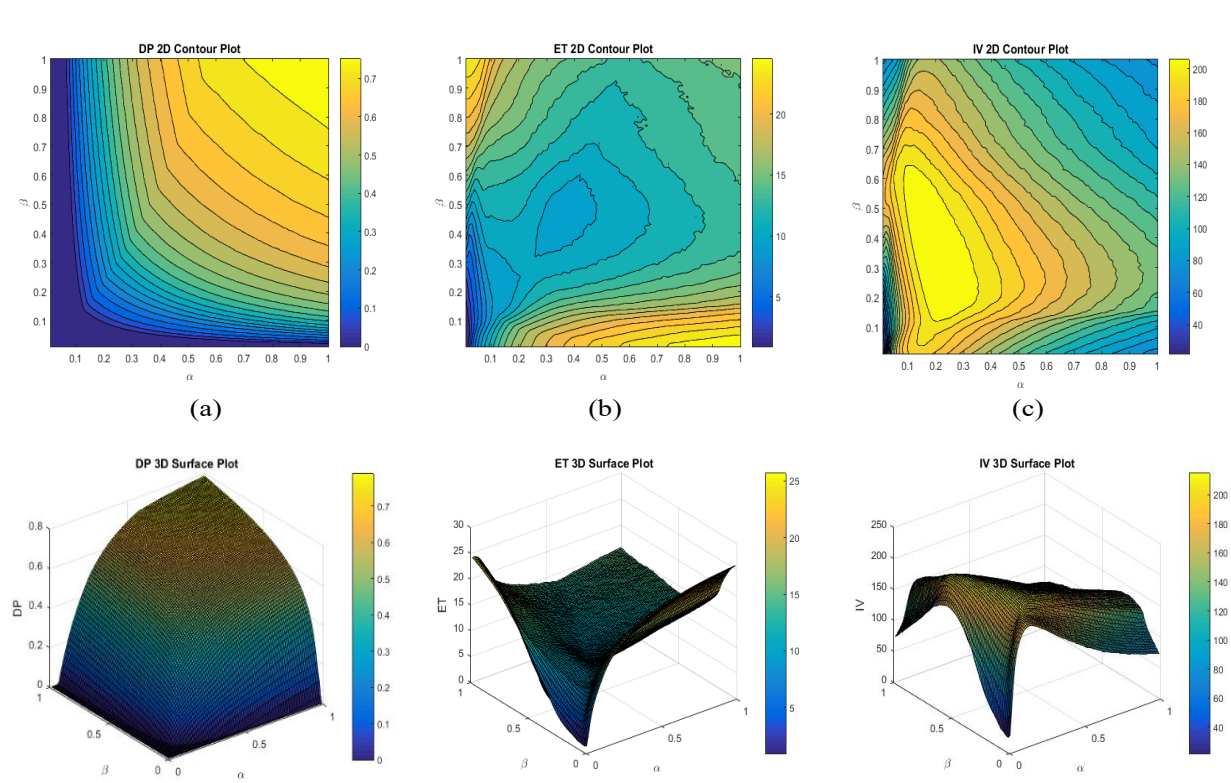


Figure 11. ET, DP and IV for Mandelbrot sets.

In **Figure 12**, Escape Time (ET), Density of Non-Escaping Points (DP), and Iteration Variance (IV) measure plots are presented for the combination of the parameters a = 0.5 and r = 2. The maximum ET value of 25.6804 is observed at $\alpha = 1.0$, $\beta = 0.01$, while the minimum ET value of 0.9364 occurs at $\alpha = 0.01$, $\beta = 0.03$. The highest DP value is 0.7886, for $\alpha = 1.0$, and $\beta = 1.0$. The minimum DP value is 0, for multiple combinations of α and β . The DP and IV plots show similar patterns. The highest IV value of 214.8429

(f)



occurs at $\alpha = 0.22$, $\beta = 0.27$, and the lowest IV value of 21.7837 is observed at $\alpha = 0.01$, $\beta = 0.03$.

Figure 12. ET, DP and IV for Mandelbrot sets.

(e)

(d)

In **Figure 13**, Escape Time (ET), Density of Non-Escaping Points (DP), and Iteration Variance (IV) measures plots are shown for the combination of the parameters a = 0.5 and r = 4. The maximum number of Picard-S3 iteration is set to 30, and the plotting area is $[-2,2] \times [-2,2]$. It is observed that the highest ET value, 22.0562, occurs at $\alpha = 0.01$, $\beta = 1.0$, while the lowest ET value, 4.3802, is observed at $\alpha = 0.10$, $\beta = 0.18$. The DP plot show a different functioning compared to the ET measure on comparison. The highest DP value of 0.8878 occurs at $\alpha = 1.0$, $\beta = 1.0$, and the minimum DP value of 0.6 is recorded at $\alpha = 0.01$, $\beta = 0.01$. The plots of DP and IV shows different trends. The highest IV value, 191.6480, is observed at $\alpha = 0.01$, $\beta = 0.05$, and the lowest IV value of 47.5911 occurs at $\alpha = 1.0$, $\beta = 0.98$.

In **Figure 14**, the Escape Time (ET), Density of Non-Escaping Points (DP), and Iteration Variance (IV) plots are presented for the parameters a = 0.5 and r = 7. From the plots, it is observed that the maximum ET value, 19.4684, occurs at $\alpha = 0.01$, $\beta = 1.0$, while the minimum ET value, 1.7784, is recorded at $\alpha = 0.01$, $\beta = 0.05$. The DP plot shows distinct characteristic compared to the ET measure. The highest DP value of 0.9104 occurs at $\alpha = 1.0$, $\beta = 1.0$, and the lowest DP value of 0.7808 at $\alpha = 0.01$, $\beta = 0.01$. The plots of DP and IV show similar trends. The highest IV value, 144.6103, is observed at $\alpha = 0.01$, $\beta = 0.04$, while the lowest IV value, 41.5881, occurs at $\alpha = 1.0$, $\beta = 1.0$.

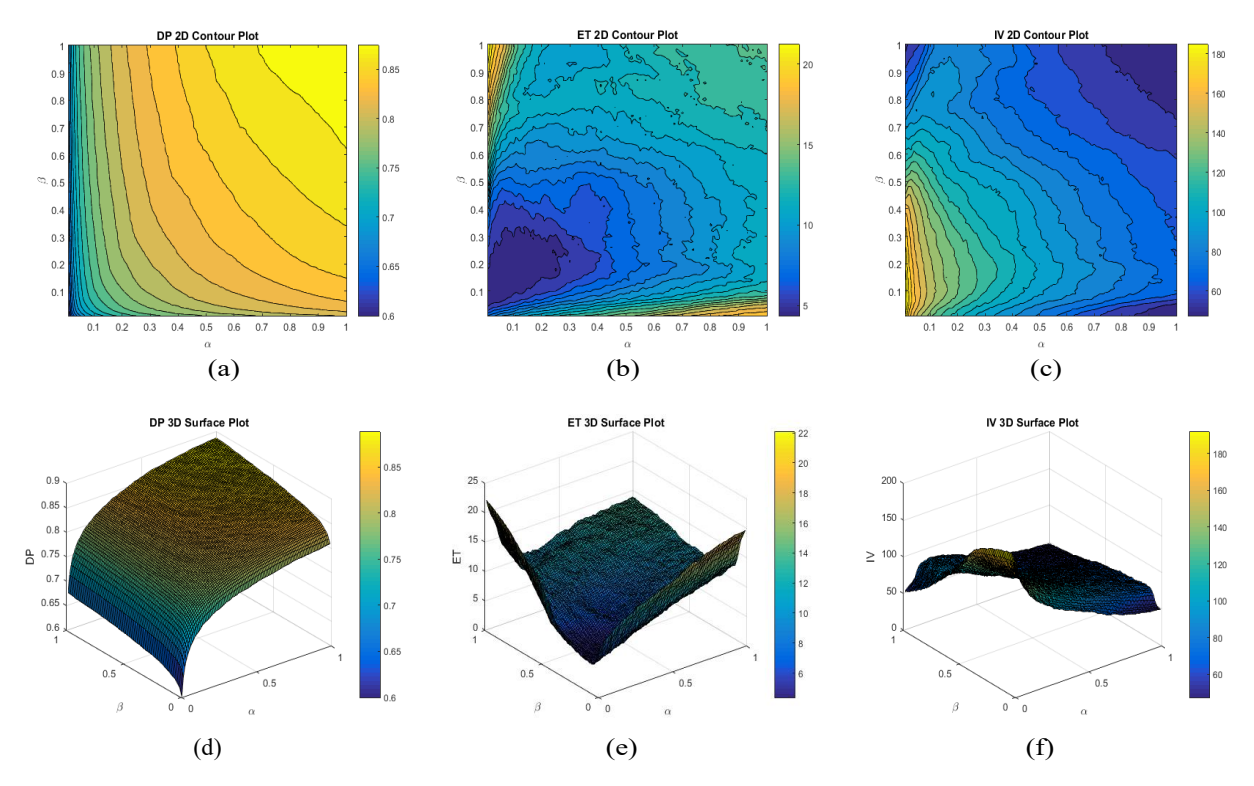


Figure 13. ET, DP and IV for Mandelbrot sets.

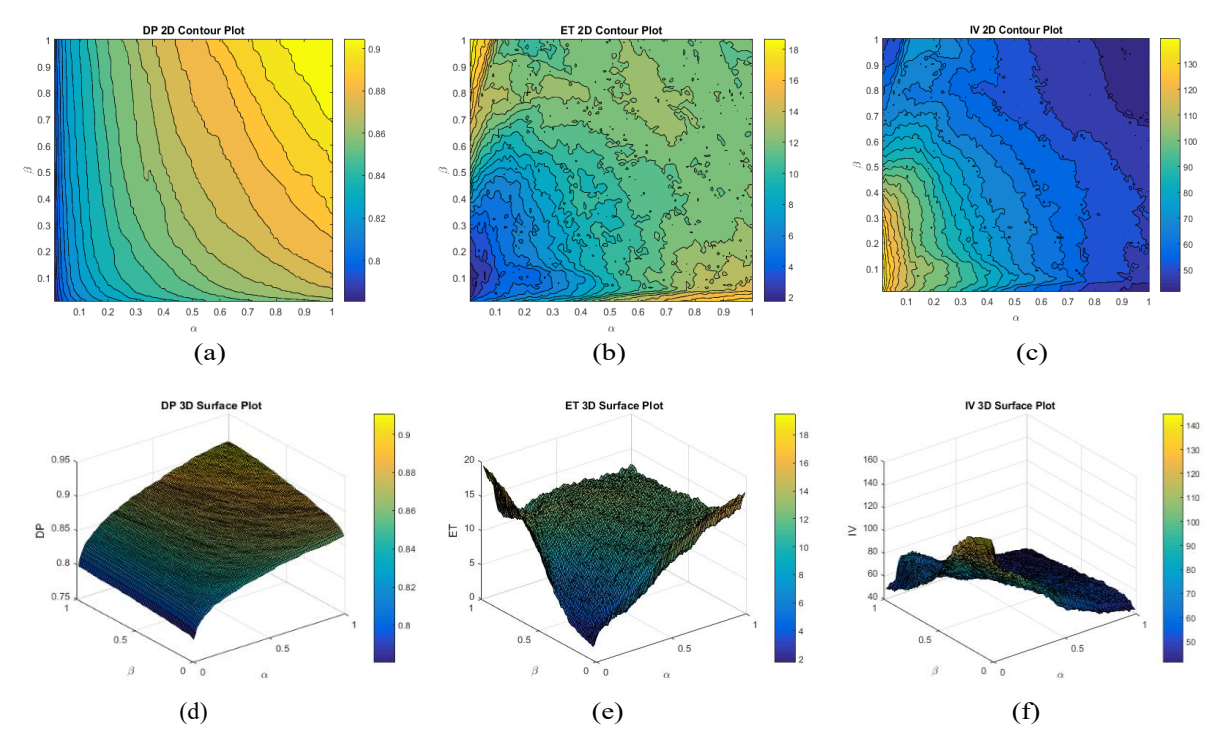


Figure 14. ET, DP and IV for Mandelbrot sets.

In **Figure 15**, the Escape Time (ET), Density of Non-Escaping Points (DP), and Iteration Variance (IV) measures plots are presented for the parameters a = 0.5 and r = 15. From the plots, it is observed that the maximum ET value, 19.4877, occurs at $\alpha = 0.01$, $\beta = 1.0$, while the minimum ET value, 1.8541, is recorded at $\alpha = 0.01$, $\beta = 0.06$. The DP plot shows a distinct behavior contrast to the ET measure. The highest DP value of 0.9320 at numerous values of α and β , while the minimum DP value, 0.8280, occurs at $\alpha = 0.01$, $\beta = 0.01$. DP and IV plots show similar trends. The highest IV value, 119.8681, occurs at $\alpha = 0.01$, $\beta = 0.06$, and the lowest IV value, 38.2918, is observed at $\alpha = 0.98$, $\beta = 1.0$.

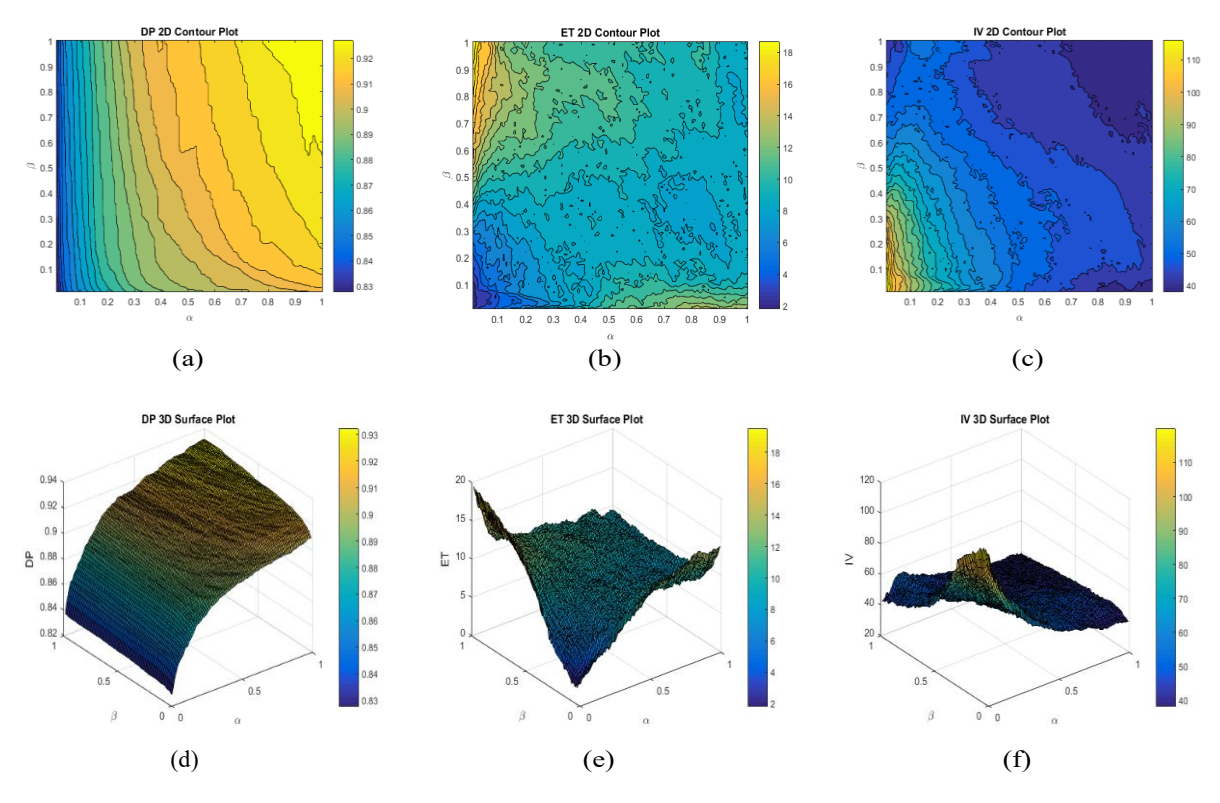


Figure 15. ET, DP and IV for Mandelbrot sets.

6. Conclusion and Future Scope

The escape criteria for the second-degree complex polynomial function $T(x) = x^r + ax + c$, where c and a are complex numbers and $r \ge 2$, has been derived using the Picard-S3 Iteration method. By leveraging Theorem 3.1 and Corollary 3.1 in the Picard-S3 orbit, both Mandelbrot and Julia sets have been visualized and analyzed. The results provide a detailed analysis of the Mandelbrot and Julia sets produced for different values of r. We found that as r varies, so do the distribution and quantity of attractors and repellers. The boundary of the Julia set is complex for distinct values of c, while the Mandelbrot set begins to resemble petals as r increases. Additionally, the escape time for fractal generation was calculated, and it varies according to the parameters that are used in the Julia and Mandelbrot sets. These images were created using a variety of techniques, which affected their color schemes, dynamics, and general appeal. Figures 5(d)-(f) resemble to flower petals and star-like shapes for higher values of r. Values of numerical measures Escape Time (ET), Density of Non-Escaping Points (DP), and Iteration Variance (IV) are maximum and minimum at the boundary of the parametric space. These findings show the effect of different numerical methods on the generation of fractals.

For future scope, exploring fractional or higher-degree complex polynomials for Picard-S3 iteration could result in the finding of more complex and different fractal structures such as biomorphs. Examining different iterative techniques such as hybrid Picard iteration, M iteration, T iteration, etc., and combining them with Picard-S3 iteration to analyze convergence, efficiency, and the impact of the resulting fractals can be useful. Further effects of various parameters present in iteration schemes may also give insight into fractal's symmetry, stability, and bifurcation analysis. Additionally, there is a possibility of creating computationally efficient real-time visualization methods that could be applied in various fields like computer graphics, system simulation, and interactive learning environments. Given the intricacy of these fractals, multifractal analysis may be an effective method for examining structural variations at various scales.

Conflict of Interest

The authors confirm that there is no conflict of interest to declare for this publication.

Acknowledgments

This research did not receive any specific grant from funding agencies in the public, commercial, or not-for-profit sectors. The authors would like to thank the editor and anonymous reviewers for their comments that help improve the quality of this work.

AI Disclosure

The author(s) declare that no assistance is taken from generative AI to write this article.

References

- Abbas, M., Iqbal, H., & De la Sen, M. (2020). Generation of Julia and Mandelbrot sets via fixed points. *Symmetry*, 12(1), 86. https://doi.org/10.3390/sym12010086.
- Adhikari, N., & Sintunavarat, W. (2024). Exploring the Julia and Mandelbrot sets of z^p+ logc^t using a four-step iteration scheme extended with s-convexity. *Mathematics and Computers in Simulation*, 220, 357-381. https://doi.org/10.1016/j.matcom.2024.01.010.
- Antal, S., Tomar, A., Prajapati, D.J., & Sajid, M. (2021). Fractals as Julia sets of complex sine function via fixed point iterations. *Fractal and Fractional*, *5*(4), 272. https://doi.org/10.3390/fractalfract5040272.
- Barcellos, A. (1990). Fractals everywhere. by Michael barnsley. *The American Mathematical Monthly*, 97(3), 266-268. https://doi.org/10.1080/00029890.1990.11995589.
- Devaney, R.L. (2018). A first course in chaotic dynamical systems: theory and experiment. CRC Press. Boca Raton.
- Husain, A., Nanda, M.N., Chowdary, M.S., & Sajid, M. (2022). Fractals: an eclectic survey, part-I. *Fractal and Fractional*, *6*(2), 89. https://doi.org/10.3390/fractalfract6020089.
- Julia, G. (1918). Mémoire sur l'itération des fonctions rationnelles. *Journal de Mathématiques Pures et Appliquées*, 1, 47-245.
- Mandelbrot, B.B. (1982). The fractal geometry of nature. W.H. Freeman and Company, New York.
- Noor, M.A. (2000). New approximation schemes for general variational inequalities. *Journal of Mathematical Analysis and Applications*, 251(1), 217-229. https://doi.org/10.1006/jmaa.2000.7042.
- Özgür, N., Antal, S., & Tomar, A. (2022). Julia and Mandelbrot sets of transcendental function via Fibonacci-Mann iteration. *Journal of Function Spaces*, 2022(1), 2592573. https://doi.org/10.1155/2022/2592573.
- Prajapati, D.J., Rawat, S., Tomar, A., Sajid, M., & Dimri, R.C. (2022). A brief study on Julia sets in the dynamics of entire transcendental function using Mann iterative scheme. *Fractal and Fractional*, *6*(7), 397. https://doi.org/10.3390/fractalfract6070397.



- Qi, H., Tanveer, M., Nazeer, W., & Chu, Y. (2020). Fixed point results for fractal generation of complex polynomials involving sine function via non-standard iterations. *IEEE Access*, 8, 154301-154317.
- Shahid, A.A., Nazeer, W., & Gdawiec, K. (2021). The Picard–Mann iteration with s-convexity in the generation of Mandelbrot and Julia sets. *Monatshefte für Mathematik*, 195, 565-584. https://doi.org/10.1007/s00605-021-01591-z.
- Sharma, S., Padaliya, S.K., & Tomar, A. (2023). Fractals as Julia and Mandelbrot sets of logarithmic function using Dogan and Karakaya (DK) iterative scheme. *Annals of Science and Allied Research*, *1*, 129-140. https://doi.org/10.5281/zenodo.10525972.
- Sharma, S., Tomar, A., & Padaliya, S.K. (2025). On the evolution and importance of the Fibonacci sequence in visualization of fractals. *Chaos, Solitons & Fractals*, 191, 115851. https://doi.org/10.1016/j.chaos.2024.115851.
- Shatanawi, W., Bataihah, A., & Tallafha, A. (2020). Four-step iteration scheme to approximate fixed point for weak contractions. *Computers, Materials & Continua*, 64, 1491-1504.
- Singh, P., Singh, V., & Singh, S. (2022). Introducing the Picard-S3 iteration for fixed points. *Australian Journal of Mathematical Analysis and Applications*, 19(2), 1-13.
- Srivastava, R., Tassaddiq, A., & Kasmani, R.M. (2024). Escape criteria using hybrid Picard S-iteration leading to a comparative analysis of fractal Mandelbrot sets generated with S-iteration. *Fractal and Fractional*, 8(2), 116. https://doi.org/10.3390/fractalfract8020116.
- Tassaddiq, A., Tanveer, M., Azhar, M., Arshad, M., & Lakhani, F. (2023). Escape criteria for generating fractals of complex functions using DK-iterative scheme. *Fractal and Fractional*, 7(1), 76.https://doi.org/10.3390/fractalfract7010076.
- Tomar, A., Antal, S., Prajapati, D.J., & Agarwal, P. (2022). Mandelbrot fractals using fixed-point technique of sine function. In *Proceedings of the Institute of Mathematics and Mechanics, National Academy of Sciences of Azerbaijan* (Vol. 48, pp. 194-214). https://doi.org/10.30546/2409-4994.48.2022.194214.
- Tomar, A., Kumar, V., Rana, U.S., & Sajid, M. (2023). Fractals as Julia and Mandelbrot sets of complex cosine functions via fixed point iterations. *Symmetry*, 15(2), 478. https://doi.org/10.3390/sym15020478.
- Weibel, E.R. (1991). Fractal geometry: a design principle for living organisms. *American Journal of Physiology-Lung Cellular and Molecular Physiology*, 261(6), L361-L369. https://doi.org/10.1152/ajplung.1991.261.6.L361.



Original content of this work is copyright © Ram Arti Publishers. Uses under the Creative Commons Attribution 4.0 International (CC BY 4.0) license at https://creativecommons.org/licenses/by/4.0/

Publisher's Note- Ram Arti Publishers remains neutral regarding jurisdictional claims in published maps and institutional affiliations.